

A Realistic Simulation Framework for Analog/Digital Neuromorphic Architectures

Fernando M. Quintana^{1,2,3†}, **Maryada**⁴, **Pedro L. Galindo**³, **Elisa Donati**⁴,
Giacomo Indiveri⁴, **Fernando Perez-Peña**³

¹ Bio-Inspired Circuits and Systems Lab, Zernike Institute for Advanced Materials, University of Groningen, Netherlands

² Groningen Cognitive Systems and Materials Center, University of Groningen, Netherlands

³ School of Engineering, University of Cádiz, Puerto Real, Cádiz, Spain

⁴ Institute of Neuroinformatics, University of Zurich and ETH Zurich, Zurich, Switzerland

E-mail: f.m.quintana.velazquez@rug.nl

September 2024

Abstract. Developing dedicated neuromorphic computing platforms optimized for embedded or edge-computing applications requires time-consuming design, fabrication, and deployment of full-custom neuromorphic processors. To ensure that initial prototyping efforts, exploring the properties of different network architectures and parameter settings, lead to realistic results it is important to use simulation frameworks that match as best as possible the properties of the final hardware. This is particularly challenging for neuromorphic hardware platforms made using mixed-signal analog/digital circuits, due to the variability and noise sensitivity of their components. In this paper, we address this challenge by developing a software spiking neural network simulator explicitly designed to account for the properties of mixed-signal neuromorphic circuits, including device mismatch variability.

The simulator, called **ARCANA** (**A** Realistic **S**imulation **F**ramework for **A**nalog/**D**igital **N**euro**M**orphic **A**rchitectures), is designed to reproduce the dynamics of mixed-signal synapse and neuron electronic circuits with autogradient differentiation for parameter optimization and GPU acceleration. We demonstrate the effectiveness of this approach by matching software simulation results with measurements made from an existing neuromorphic processor. We show how the results obtained provide a reliable estimate of the behavior of the spiking neural network trained in software, once deployed in hardware. This framework enables the development and innovation of new learning rules and processing architectures in neuromorphic embedded systems.

Keywords: SNN, DPI, neuromorphic, PyTorch, DYNAP-SE

1. Introduction

Mixed-signal neuromorphic circuits emulate the neural and synaptic dynamics observed in real neural systems, reproducing features such as limited precision, heterogeneity, and high

† Corresponding author

sensitivity to noise [4, 13], which are often considered not ideal in Artificial Intelligence (AI) workloads. Indeed, software simulations of spiking neural networks in AI typically use bit-precise identical activation functions for all neurons in the network and highly precise and high-resolution parameters. Conversely, in the domain of computational neuroscience, neuron and spiking neural networks simulation engines, such as “Neuron” and “NEST” take into account more realistic properties of real neurons, including variability and stochasticity [7, 8, 23]. However, these simulators do not account for many of the properties of the electronic circuits used to emulate real neurons and synapses. In this paper, we bridge this gap by introducing a simulation platform, *ARCANA*, for mixed-signal neuromorphic systems, optimized to simulate neurons and synapses using differential equations derived from their electronic circuit models. By integrating this framework with the PyTorch simulator, not only simulations but also optimization of parameters can be offered to the user for the final deployment of the network in hardware. This enables neuromorphic engineers, computational neuroscientists and AI application developers to test and validate spiking neural network architectures in a fast prototyping environment before testing the final system in the field, in a real-world application scenario [11, 16, 19, 22, 25].

A hardware-aware trained network can be effortlessly deployed on an inference chip like those of the DYNAP family [15, 20]. The simulator can be easily adapted to incorporate hardware-specific constraints during model training, enabling a unified framework for various platforms. This approach provides two significant advantages: (1) it simplifies the transfer of a single model across multiple platforms, ensuring seamless cross-platform deployment and (2) it makes it feasible to benchmark different hardware using various datasets. Additionally, if a chip supports on-chip learning, deploying a pre-trained network allows it to continuously learn and adapt to new real-world data.

2. Methods

The mixed signal circuit equations that we used for this framework are the ones based on the Differential Pair Integrator (DPI) circuit [1], commonly used to implement both synapse and neuron circuits [4, 12, 14, 17, 21, 24]. The DPI synapse equations reproduce faithfully realistic synaptic dynamics [1] and the equations of the corresponding neuron reproduce the behavior of the Adaptive Exponential Integrate & Fire (AdExI&F) neuron model [2]. As DPI is a current-mode log-domain filter, both the synapse and the internal variables of the neurons are expressed as *currents*, even though in theoretical and computational models, the neuron variable is the membrane *potential*. In the simulator, we use terminology and variable names that match those of the electronic circuits as closely as possible.

The mixed-signal neuromorphic processor used to validate the simulations is the Dynamic Neuromorphic Asynchronous Processor (DYNAP-SE) [15]. It is a multi-core spiking processor with four cores with 256 neurons per core, providing a total of 1024 neurons [15].

2.1. DPI synapse

The dynamic behavior of the circuit can be approximated as a first-order differential in equation [5]:

$$\tau \frac{d}{dt} I_{syn} + I_{syn} = \frac{I_g}{I_\tau} I_w \quad (1)$$

where $\tau = CU_T/\kappa I_\tau$ is the synapse decay time constant, I_g the DPI filter gain, and I_w the synaptic weight.

The simulator can model four different types of synapses, two excitatory synapses (AMPA and NMDA) and two inhibitory (GABA_a and GABA_b): (1) **AMPA synapse** which is composed of a DPI block and is connected directly to the input of the neuron, modeling biological AMPA synapses; (2) An **NMDA synapse** shares similarities with AMPA-style synapses in that they are both excitatory synapses directly linked to inputs. However, unlike AMPA synapses, NMDA synapses incorporate a pair of differential blocks to introduce a voltage gating mechanism. This mechanism makes the synaptic current dependent on the neuron's membrane potential reaching a specific threshold; (3) **GABA_a synapse** are inhibitory synapse that implements a mirror current to subtract current from the input of the neuron, and (4) **GABA_b synapse** with very similar behavior to GABA_a, but with the difference that the current mirror is connected directly to the membrane current instead of to the input of the neuron, increasing the neuron leakage.

2.2. The DPI neuron

The DPI neuron circuit comprises four main blocks:

- **Input DPI model leak** integrates the DPI inputs coming from the synapses and the DC input current, charging the capacitor C_{mem} that models the neuron leak conductance. It has a series of transistors that control the input current gain, DC input current, and leakage current that discharges the capacitor. The current is composed of the constant DC current and the current coming from the two excitatory synapses *AMPA* and *NMDA*, as well as the inhibitory synapse *GABA_a*, which subtracts the current directly from the input. Moreover, the *GABA_b* synapse is connected to the leakage current, directly discharging the capacitor.
- **After-HyperPolarization (AHP) block** is a slow negative feedback block that models spike frequency adaptation. When a postsynaptic spike occurs, it integrates it into a recurrent negative after-hyper-polarizing (AHP) current, which is subtracted from the input, effectively suppressing the activity of the neuron.
- **Positive feedback and Spike generation block** that mimics sodium activation and inactivation channels. It consists of a positive feedback circuit. When the neuron current starts to spike, the current used to switch the inverter circuits is copied back into the capacitor C_{mem} , thus further increasing the neuron's internal membrane potential variable. At this point, I_{mem} current grows exponentially until the inverter circuits finish switching, at which the spike occurs and the reset block is activated.

- **Reset block** that mimics the potassium channels. The spike is reset by creating a short circuit to ground that discharges the neuron's membrane capacitance and causes the membrane potential variable I_{mem} to flow directly to ground, for a period of time controlled by a bias parameter. In this period C_{mem} cannot be re-charged and a refractory period and an absolute reset occur. After this period ends the I_{mem} current recharges the capacitor C_{mem} and the neuron returns to integrating its input spikes.

Taking into account the different blocks of which the circuit is composed, the neuron can be modeled using the following equations [5]:

$$\left(1 + \frac{I_g}{I_{mem}}\right) \tau \frac{d}{dt} I_{mem} + I_{mem} \left(1 + \frac{I_{ahp}}{I_\tau}\right) = I_\infty + f(I_{mem}) \quad (2a)$$

$$\tau_{ahp} \frac{d}{dt} I_{ahp} + I_{ahp} = I_{ahp\infty} u(t) \quad (2b)$$

$$I_\infty = \frac{I_g}{I_\tau} (I_{in} - I_{ahp} - I_\tau) \quad (2c)$$

where I_{mem} is the subthreshold current equivalent to the membrane potential of a neuron. κ the sub-threshold slope factor, I_{ahp} the current responsive of the spike-frequency adaptation. I_∞ is the maximum current that the neuron would reach asymptotically. I_τ the leakage current of the neuron, τ the neuron time constant, and I_{in} the neuron's total input current coming from the synapses and the constant DC input.

The term $f(I_{mem})$ in equation 2.2 represents the positive feedback current, which depends on the membrane current I_{mem} , and can be well fitted with an exponential function [9]:

$$f(I_{mem}) = \frac{I_{fb}}{I_\tau} (I_{mem} - I_g) \quad I_{fb} = \frac{I_0^{\frac{1}{\kappa+1}} I_{mem}^{\frac{\kappa}{\kappa+1}}}{1 + e^{-\alpha(I_{mem} - I_g)}} \quad (3)$$

Where α and I_g are adjustable parameters, I_0 dark current and κ transistor slope factor.

On-chip digital-to-analog (DAC) bias-generator circuits configure bias parameters by generating specific magnitudes of current to govern neuronal and synaptic properties, including time constant, refractory period, and synaptic weights [6]. These parameters are represented as “coarse” and a “fine” value internally, where $coarse \in [0, 7]$ and $fine \in [0, 255]$. These parameters are subject to variability as discussed in 3. Importantly, the values assigned cannot be retrieved directly from the circuits, necessitating our reliance on recording traces using an oscilloscope.

3. Hardware mismatch

Variability in analog substrate mixed-signal neuromorphic processors can lead to discrepancies when compared to idealized simulations. Typically, the coefficient of variation for these parameters is approximately 20% [26]. The values of neuron and synapse parameters are tuned to approximately match those obtained from the hardware.

Figures 1 and 2 show a distribution of τ_{mem} values for different biases set using IF_TAU1_N. The coarse value of the bias is set to 5 and we sweep the fine value ranging from 74 to 190. As

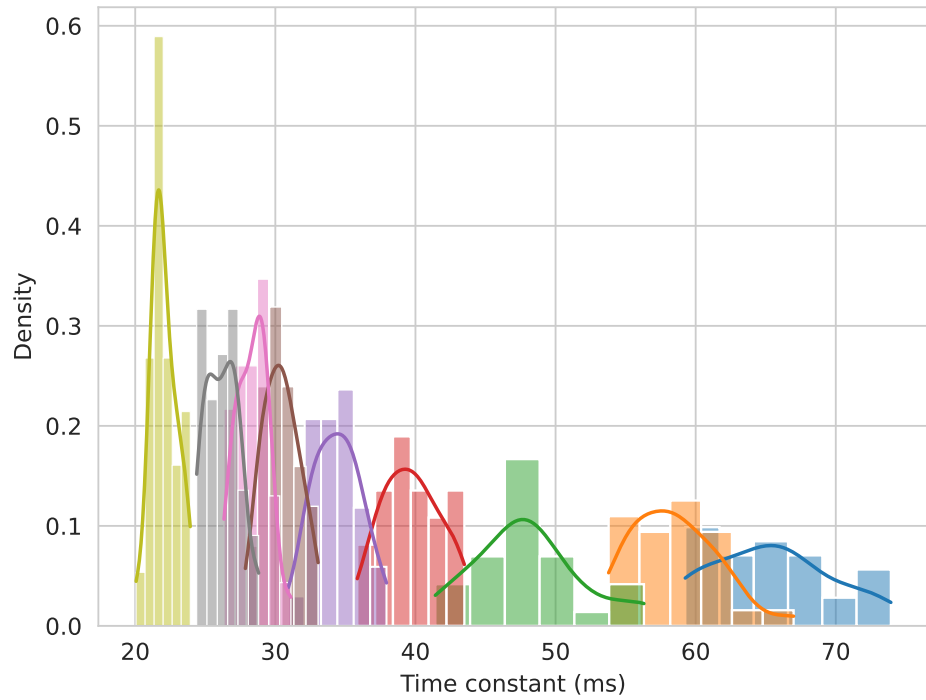


Figure 1: Time constant distribution for the time constant bias ranging from 530 nA to 1676 nA.

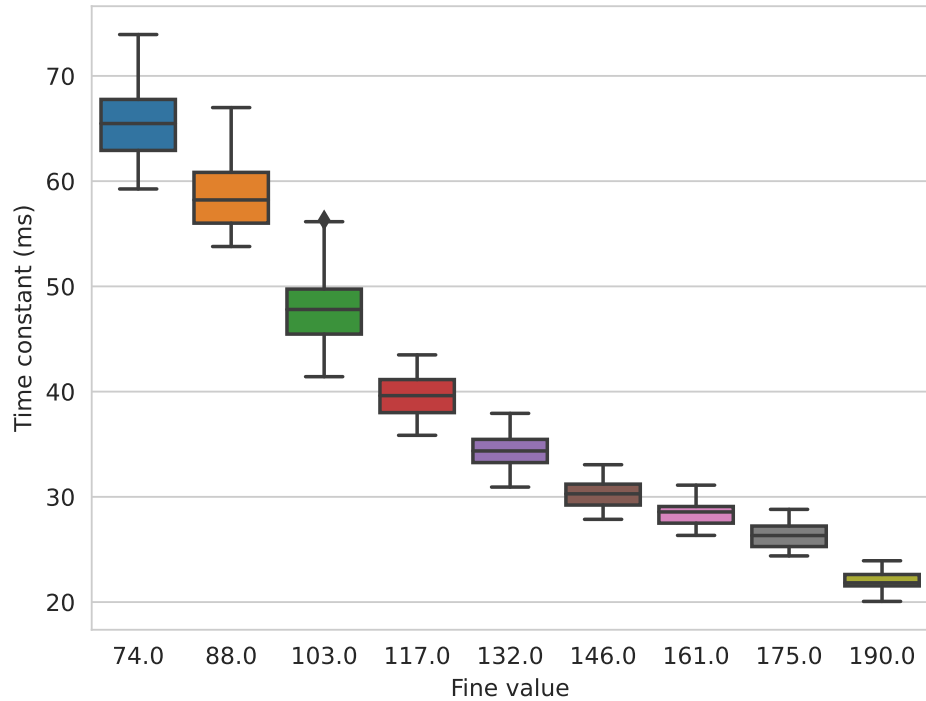


Figure 2: Time constant distribution for I_τ ranging from 530 nA to 1676 nA.

evident, the standard deviation of the values diminishes proportionally with the modified τ value. We incorporate mismatch in ARCANA in line with the observed findings. With this approach, during network training, the system becomes more resilient to hardware noise, which gives rise to mismatch.

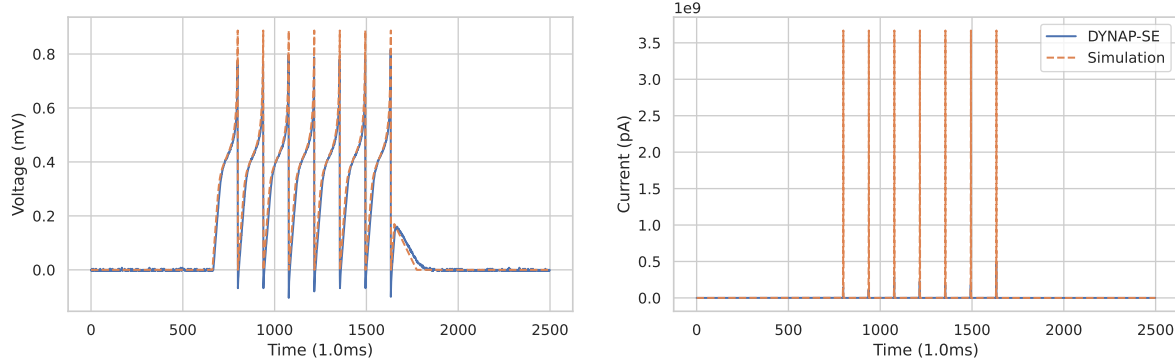
To check that the software implementation works correctly and to confirm if the neuron dynamics are very similar to those implemented on the chip, the neuron membrane potential is recorded when different parameters are changed and is compared with the simulation results (Figures 3a-3c). In each of the experiments discussed here, one of the following parameters:—constant DC input, neuron threshold, or neuron time constant— is changed to observe isolated changes in the neuron behavior. This confirms the accurate representation of these parameters in the equations and ensures that their impact on the silicon neuron’s behavior aligns with the simulation.

In Figure 3a, we compare the recorded membrane voltage traces obtained from a chip using an oscilloscope with simulation traces generated when a constant DC current is applied to the neuron. The parameters for the silicon neuron, namely the membrane time constant (I_τ), neuron gain (I_g), and the amplitude of the DC current (I_{DC}), are configured using the [coarse, fine] values of [6,22], [6,88], and [2,57], respectively. The simulation curve is calibrated to obtain their corresponding values in pA , being thus $4.1pA$, $500pA$ and $36.6pA$ for I_τ , I_g and I_{DC} respectively. We followed a similar process to obtain the synaptic parameters, which include the time constant, gain, and weight. In this scenario, we stimulate the neurons using either a *AMPA* or *GABA_a* synapse. Figures 3b and 3c illustrate the neuron response for the specified bias values: $I_\tau = [2,20]$; $I_g = [2,20]$; weight = [5,99].

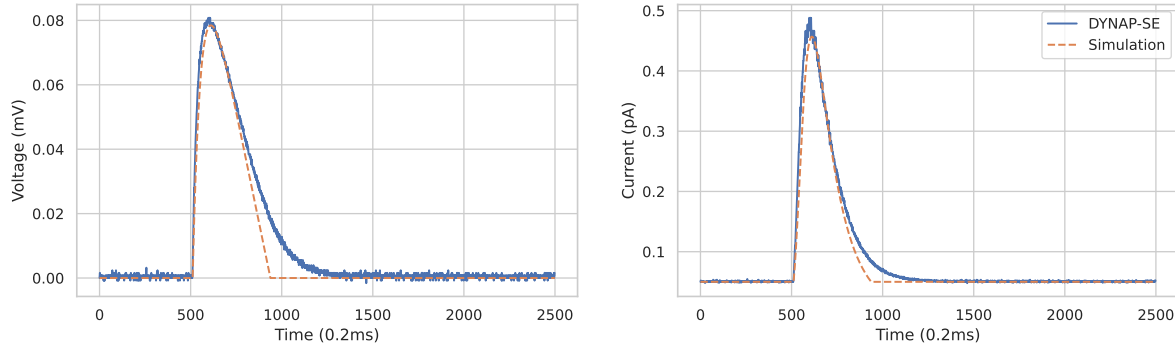
We demonstrated that ARCANA can achieve comparable dynamics in simulation with those emulated on the chip, offering a reliable assessment of the network dynamics trained in software simulation to the one deployed on the hardware. This calibration process is integrated in the later experiments (see section: 4) where three pre-trained networks were deployed on DYNAP-SE.

4. Results

We performed three experiments to assess the dynamics and accuracy of the Pytorch-based implementation of the DPI neuron and synapse model. In each experiment, the network was pre-trained using ARCANA, followed by emulation on the mixed-signal neuromorphic chip, DYNAP-SE. Our first demonstration is a simple example of a frequency resonator (see section: 4.1) employing *autograd*. Autograd is a powerful tool that automatically calculates gradients, thereby facilitating tuning and optimization of complex models. Following this, we applied a comparable method to perform a binary classification task (see section: 4.2). In the final experiment (refer to section: 4.3), we present a proof-of-concept for Event-based Three-factor Local Plasticity (ETLP) [18] emulated on the DYNAP-SE. This serves as validation for the algorithm’s compatibility with hardware-aware training. The potential to deploy pre-learned weights on mixed-signal hardware opens up exciting prospects for real-world applications in the field of mixed-signal neuromorphic chips.



(a) Comparison between ARCANA and DYNAP-SE chip using a constant DC.



(b) Comparison between ARCANA and DYNAP-SE chip using a AMPA input synapse.

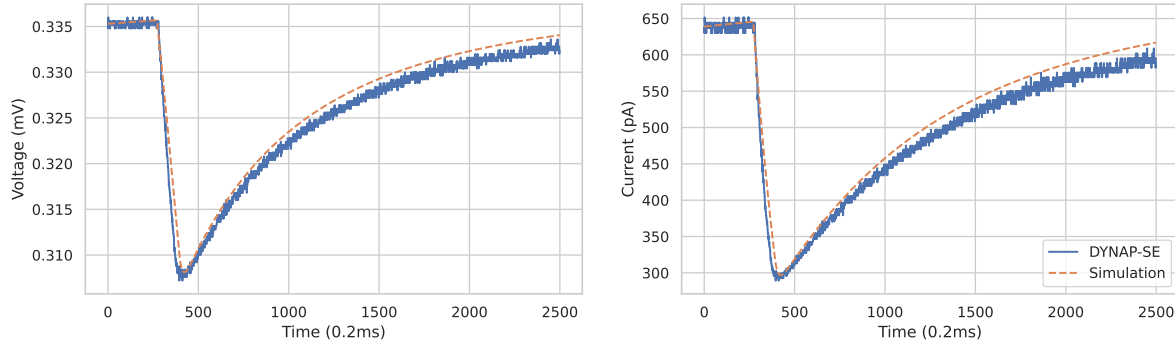
(c) Comparison between ARCANA and DYNAP-SE chip using a GABA_a input synapse.

Figure 3: ARCANA and DYNAP-SE comparison, where on each figure, the left pane represents the voltage and the right pane the soma current.

4.1. Spike frequency resonator

In this experiment, we perform a basic task to showcase the use of autograd tool to optimize neuron parameters. The task involves continuous stimulation of a neuron with a 10 pA DC. The objective is to modify neuron threshold and time constant biases to achieve the desired firing frequency. These experiments highlight the optimization of various neuronal parameters. Figure 4 (top) shows the initial response of the neuron to DC injection. The absence of a spike response indicates the need to precisely adjust the neuron's parameters, specifically the spike threshold and time constant. Rather than manually calibrating these parameters, we employ

Neuron parameters optimization

Optimizing leakage and gain currents of the neuron in order to fire 5 spikes in 2 seconds with a DC input of 10pA

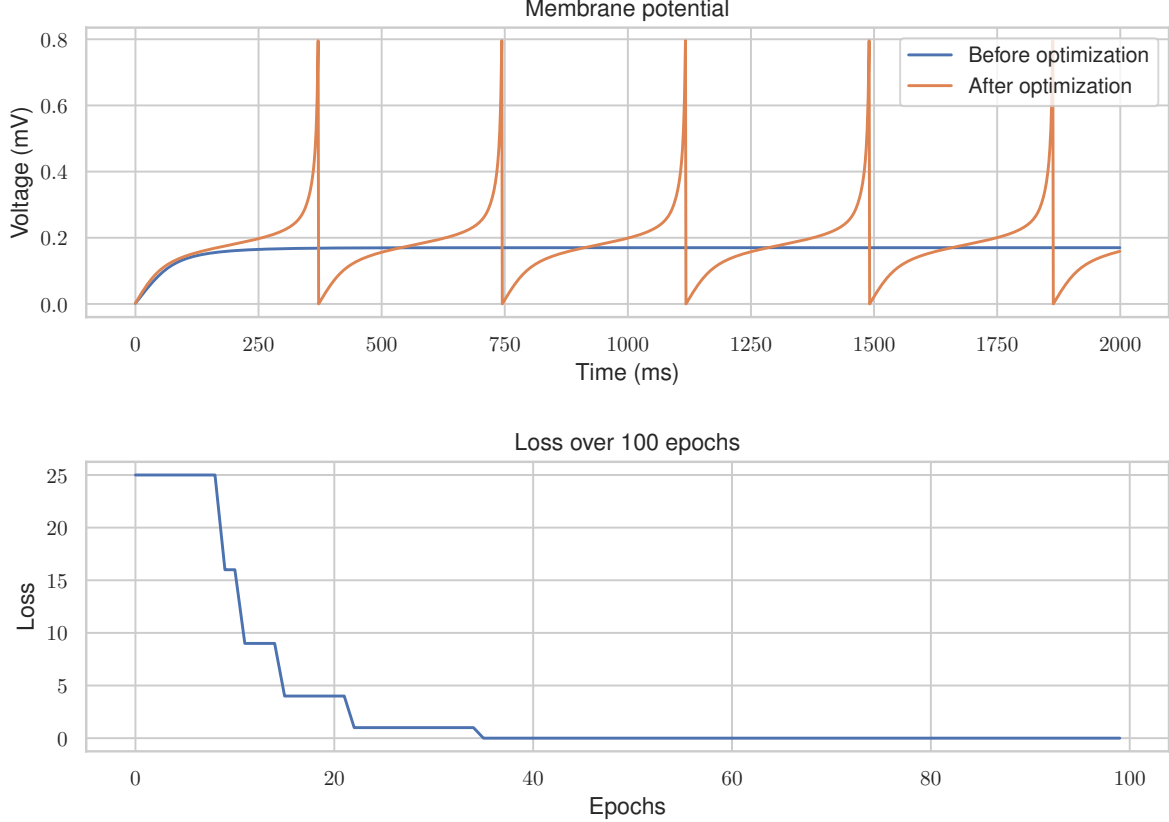


Figure 4: Neuron parameters optimization to obtain an output frequency of 2.5Hz from a constant input current of 10pA .

autograd for their automatic modification to ensure the neuron fires at the frequency specified by the user. Figure 4 (bottom) illustrates that the training process is efficiently completed in fewer than 40 epochs.

4.2. Binary Image Classification

A more complex task is to perform image classification so that a network can recognize digits. For simplicity, we only consider 0 and 1 of the MNIST dataset. This experiment involves training the weights of the network and subsequently deploying the trained network on DYNAP-SE. The aim is to ensure that the designated neuron on the chip exhibits a higher firing rate than the baseline for the digit it is selective for (0 or 1). The network receives the pixel intensity encoded as firing rate with a Poisson distribution as shown in Figure 5.

Syncing ARCANA and DYNAP-SE: To ensure a faithful deployment of a trained network, it is crucial to align the leakage and gain currents of a neuron and synapse on the mixed-signal chip and ARCANA simulator. We followed the same process as described in section 3. As

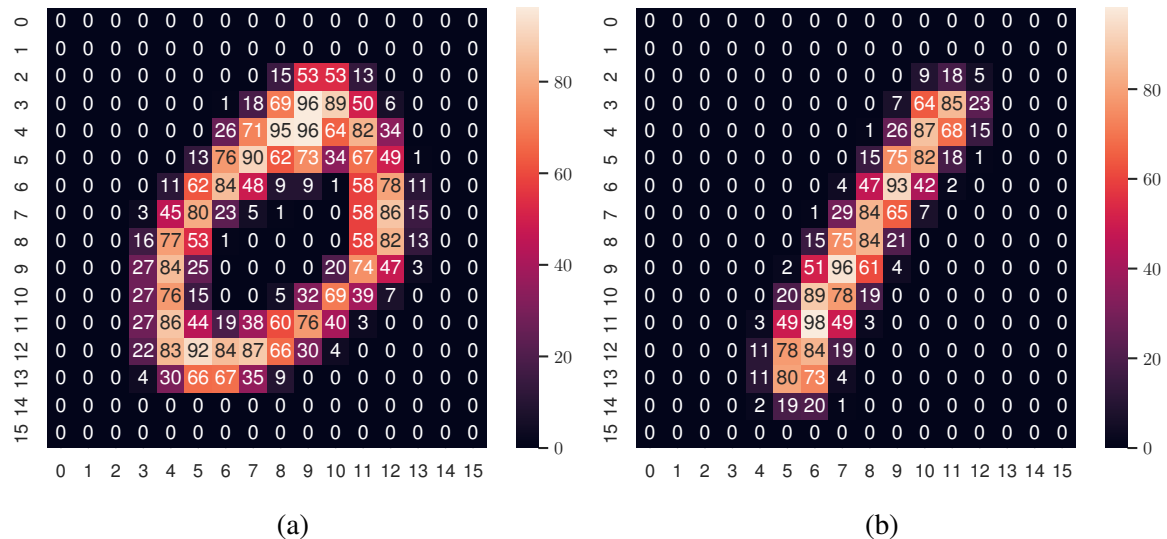


Figure 5: Samples from class 0 (A) and 1 (B) with the corresponding frequency (Hz) value to convert it into a spike train.

mentioned previously, on DYNAP-SE chip the base weight of each type of synapse (refer Section: 2.2) can be tuned using bias currents similar to other neuron and synaptic parameters. This base weight is common to all neurons in a single core. Hence, to modify the weights for a specific neuron, we alter the quantity of synapses connecting two neurons. This necessitates the quantization of the learned weight matrix into integer values. We dealt with quantization constraint by employing Quantization-Aware Training (QAT) procedure.

Network training: Considering that the classification task discussed here is linearly separable, we employ a single-layer network with 256 input channels and 2 readout neurons, with one neuron representing digit 0 and the other representing digit 1. Each neuron can receive input with multiple excitatory (AMPA) and inhibitory (GABA_a) synapses. We initialized AMPA and GABA_a weight matrices with a uniform distribution (see figure 6). Additionally, the network undergoes synaptic pruning to comply with the fan-in limitations of the neurons in DYNAP-SE.

Training weights with 32-bit floating-point arithmetic allows for a broader dynamic range. In contrast, during the inference phase, DYNAP-SE utilizes quantized weights. With the help of quantization techniques such as QAT [27], we can reduce the precision of weights from float to integer, resulting in efficient computation while maintaining high accuracy during inference on the chip. A rounding operator could be used to map the floating point tensor to a quantized representation:

$$x_q = \text{round}(x_f)$$

During training, QAT introduces a “mock” low precision in the forward pass, while the backward pass remains full precision (Figure 7). To deal with the quantization operation gradient, the Straight-Through Estimator (STE) surrogate gradient is used. This approach allows the gradient to be transmitted unaltered through the Fake-quantization operator.

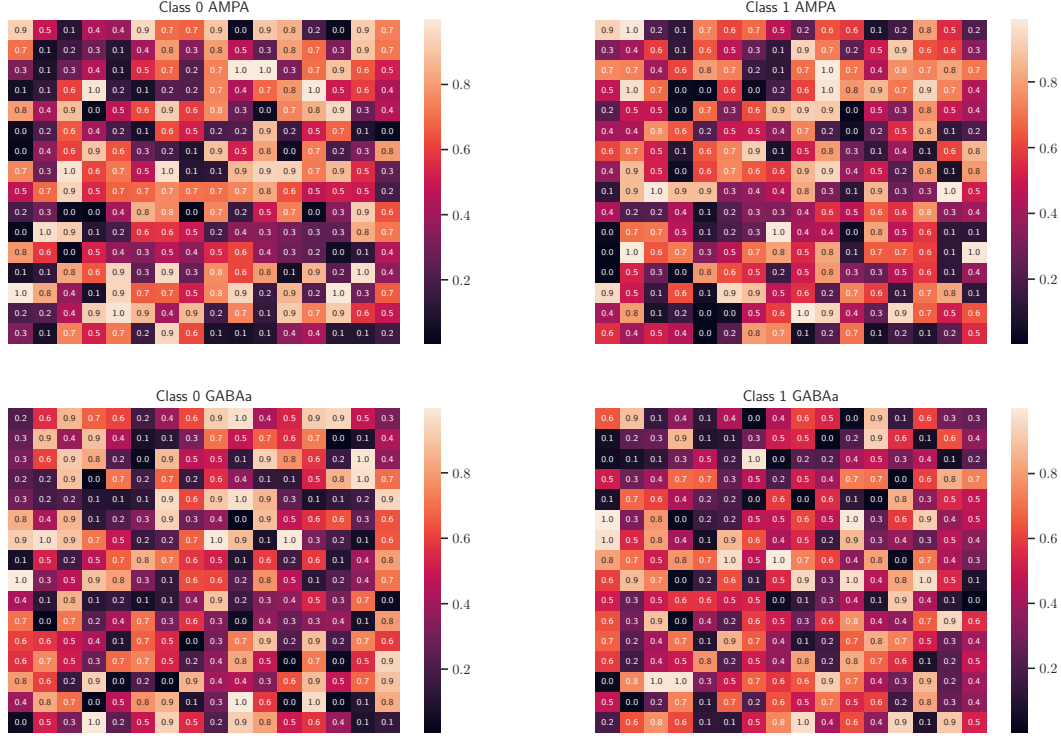


Figure 6: Initial weight matrix for AMPA and GABA_a synapses on class 0 and 1 output neurons

As previously stated, the DYNAP-SE chip also restricts the fan-in of a neuron, permitting only 64 synapses per neuron. This restriction could change depending on the chip and must be considered during training to avoid exceeding the synapse limit and risking a topology that is incompatible with the hardware. To address this challenge, we penalize the model for higher fan-in by adding L1 and/or L2 regularization terms. For instance, if W is the weight matrix and C is the desired fan-in, the regularization term could be $\lambda \sum |W - C|$, where λ is a hyperparameter that controls the strength of the regularization. If the sum of the rounded weights is not yet exactly equal to the desired value, a final adjustment can be made by adding a constant value C to each weight, defined as $C = (fanin - \sum(round(W))) / N$. Here N is the number of input neurons, and the sum is over all the input weights of each postsynaptic neuron.

The final weight matrix obtained after training (Fig. 6) is then rounded, as shown in Figure 8. Before deploying the network on the DYNAP-SE, we performed an inference mode evaluation in simulation. As anticipated, the neurons spike behavior only when exposed to their respective selective digits.

The network was deployed on the hardware as a last step in this process. During the inference phase, 2115 samples were randomly selected either of the two MNIST digits (0 or 1) from the test set and presented it to the network for 50 ms. This presentation was alternated with a rest phase of 50 ms, during which no stimulus was provided to the network (Figure 9). The firing response of the neurons was recorded for each stimulus presentation. The emulated network can correctly predict the stimulus with an accuracy of 99.11%. This demonstrates the system's feasibility for training the weights of a network in software and efficiently deploying it

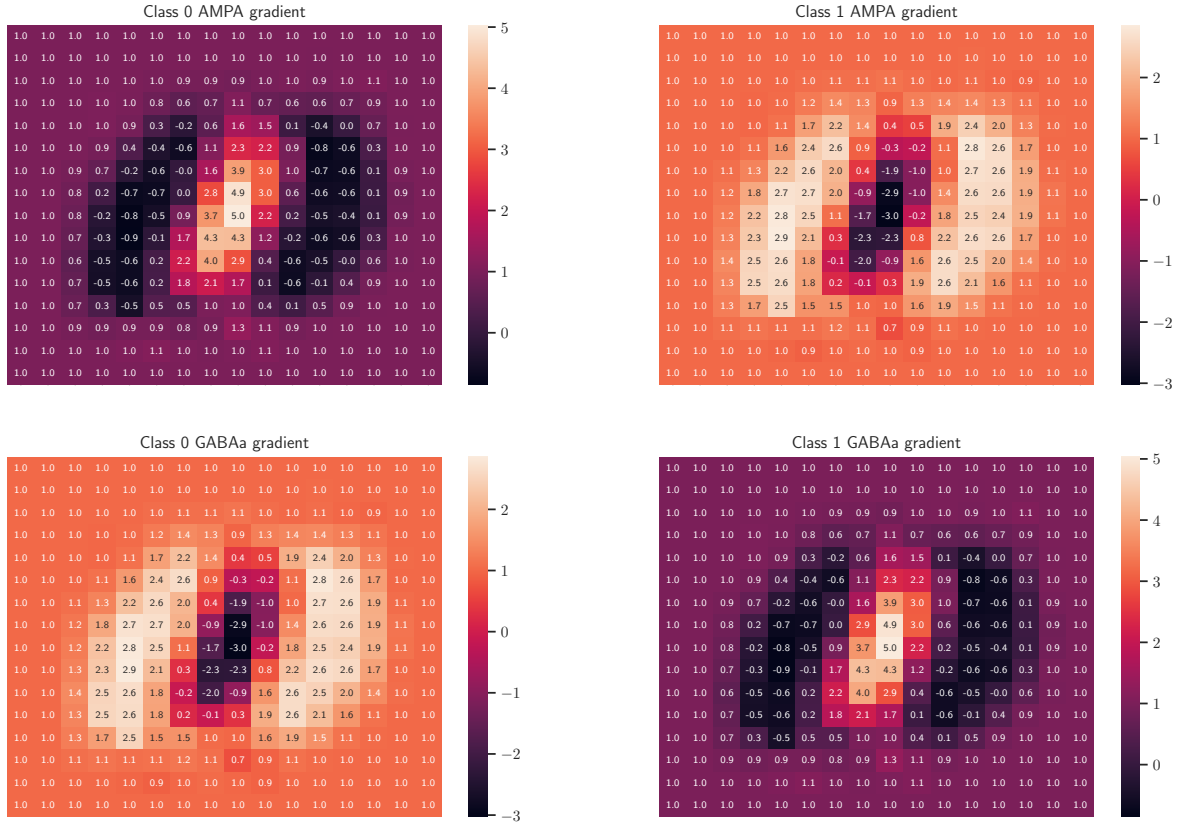


Figure 7: AMPA and GABAa synapses gradients during the training process for classes 0 and 1.

on a mixed-signal chip.

4.3. Learning rules on DYNAP-SE

In this work, we showed how ARCANA is a promising tool-chain for end-to-end network training and on-chip inference post-deployment. An important advantage of having a simulator for a mixed-signal processor such as DYNAP-SE is the possibility of testing various learning rules such as ETLP [18] with the neural model implemented in hardware. Thus, it serves as a proof-of-concept to test the viability of these learning algorithms for a specific hardware before designing the circuit layout of the learning rule for on-chip implementation.

In this final experiment, we train a network using ETLP [18]. The task consists of a synthetic dataset where the two neuron groups fire with different frequencies. Depending on which one fires, represents different classes. The network architecture has 50 input neurons, 50 hidden neurons, and 50 output neurons, with 2 teaching neurons that are firing constantly at 5Hz and 50Hz when their class is present in the training process.

Figure 10 shows the complete training and testing process on simulation, wherein the first four seconds the output neurons fire independently on the pattern presented in the network. In the next 20 seconds, both tasks are presented alternatively in the network, allowing the hidden

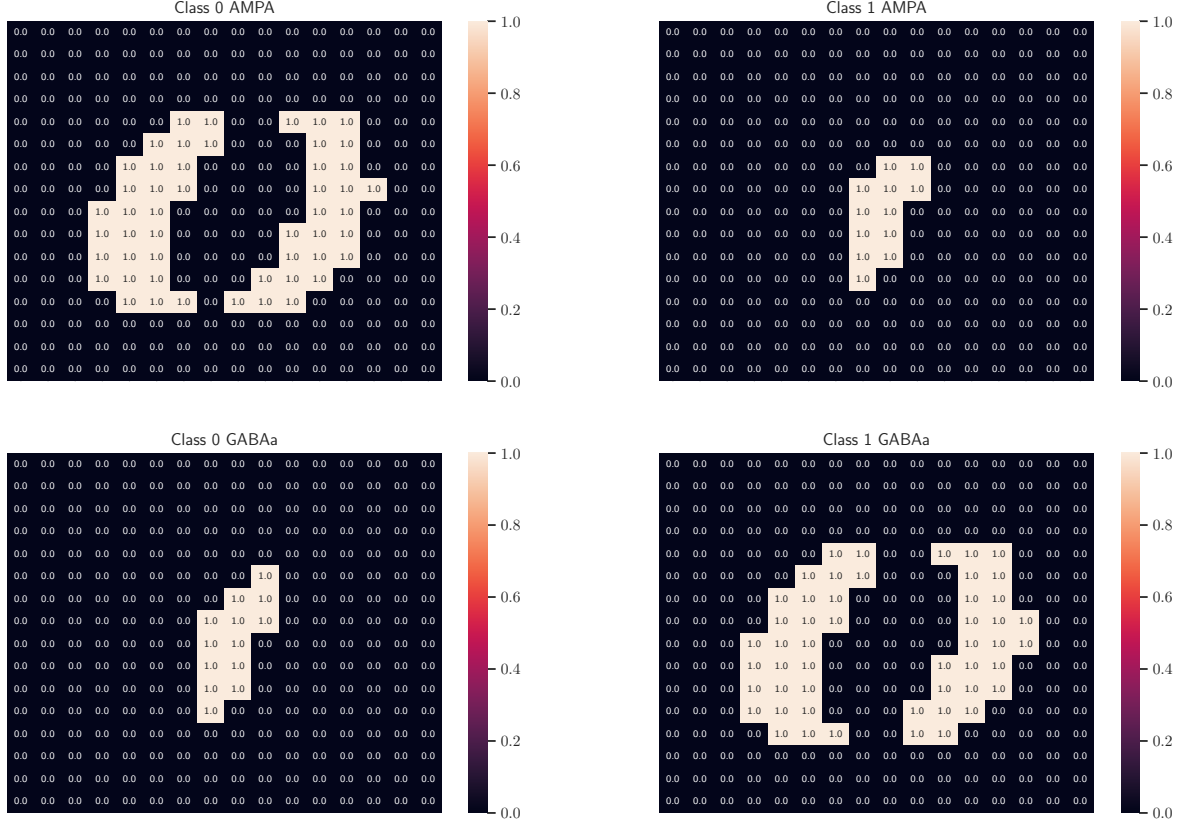


Figure 8: AMPA and GABA_a connection matrix for class 0 and 1.

and output layers to learn the relation between the classes and the input neurons. Finally, the teaching neurons are set to a low-rate firing state, showing that the output neurons fire with the correct class.

Once the network was trained, the weights were exported into a network created on DYNAP-SE without any preprocessing step. Figure 11 shows the output of the network hidden and output layers on hardware. Exhibiting the desired behavior for each individual input.

5. Discussion

In this paper, we presented the ARCANA simulator for mixed-signal hardware and validated its performance using the DYNAP-SE chip. The advantage of ARCANA is its ability to use of the PyTorch “autograd” feature, which allows the optimization of the internal parameters of the network. While other similar simulators developed in parallel to this work have been proposed within the Rockpool framework Cakal et al. [3], specifically tailored for DYNAP-SE2 chip [20], ARCANA boasts a more versatile application and is generic to any processor incorporating DPI based neuron models, independent of the specific simulation framework used. This adaptability of ARCANA is achieved by fine-tuning parameters such as the positive-feedback exponential function parameters and the chip constant values, including the transistor slope factor and neuron capacitor. Furthermore, ARCANA allows us to optimize not only the weights but

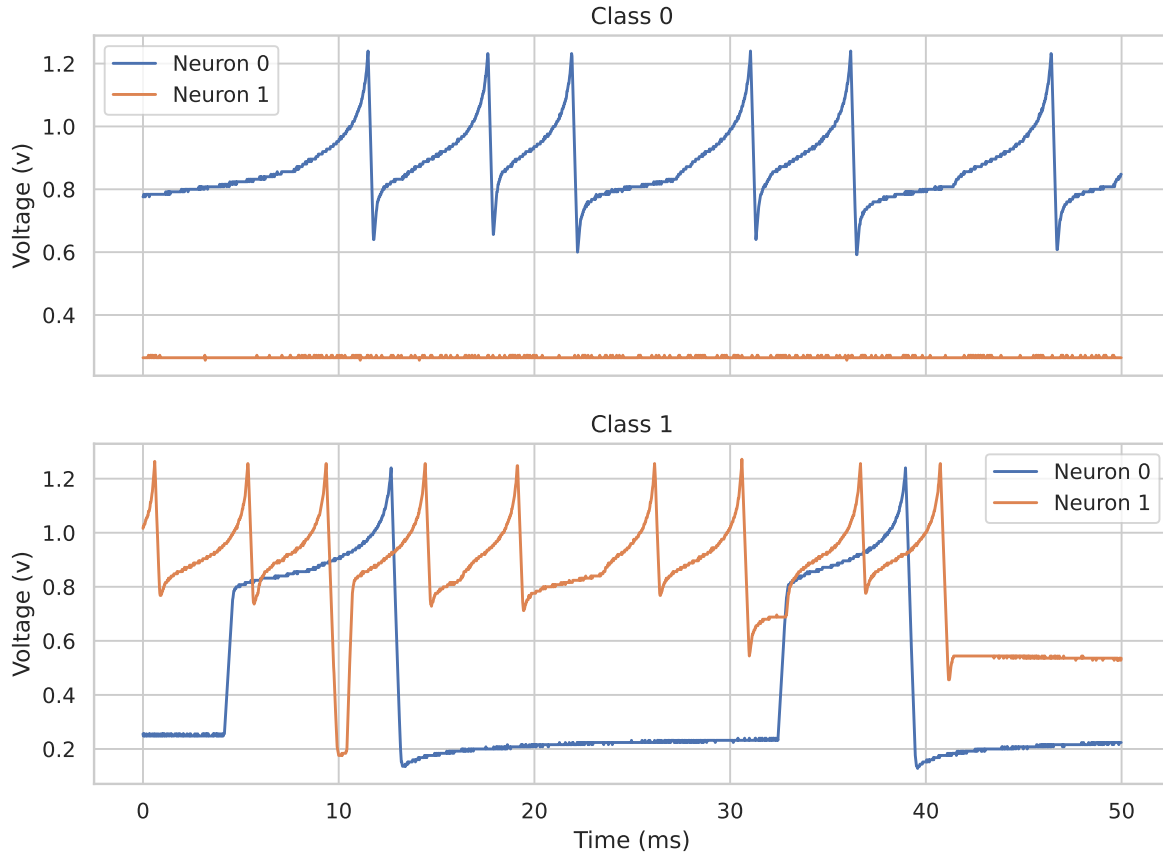


Figure 9: Output neurons voltages recorded on DYNAP-SE when receiving a sample from class 0 and class 1.

other parameters as well. Finally, we demonstrated the feasibility of implementing ETLP in hardware and to apply it to online training in mixed signal hardware. This opens new doors to the development of new local learning rules in embedded systems that go beyond the ones presented so far [10].

References

- [1] C. Bartolozzi and G. Indiveri. “Synaptic dynamics in analog VLSI”. In: *Neural Computation* 19.10 (Oct. 2007), pp. 2581–2603. doi: 10.1162/neco.2007.19.10.2581.
- [2] Romain Brette and Wulfram Gerstner. “Adaptive exponential integrate-and-fire model as an effective description of neuronal activity”. In: *Journal of neurophysiology* 94.5 (2005), pp. 3637–3642. doi: 10.1152/jn.00686.2005.
- [3] Ugurcan Cakal, Maryada, Chenxi Wu, Ilkay Ulusoy, and Dylan Richard Muir. “Gradient-descent hardware-aware training and deployment for mixed-signal neuromorphic processors”. In: *Neuromorphic Computing and Engineering* 4.1 (Mar. 2024), p. 014011. doi: 10.1088/2634-4386/ad2ec3. URL: <https://dx.doi.org/10.1088/2634-4386/ad2ec3>.

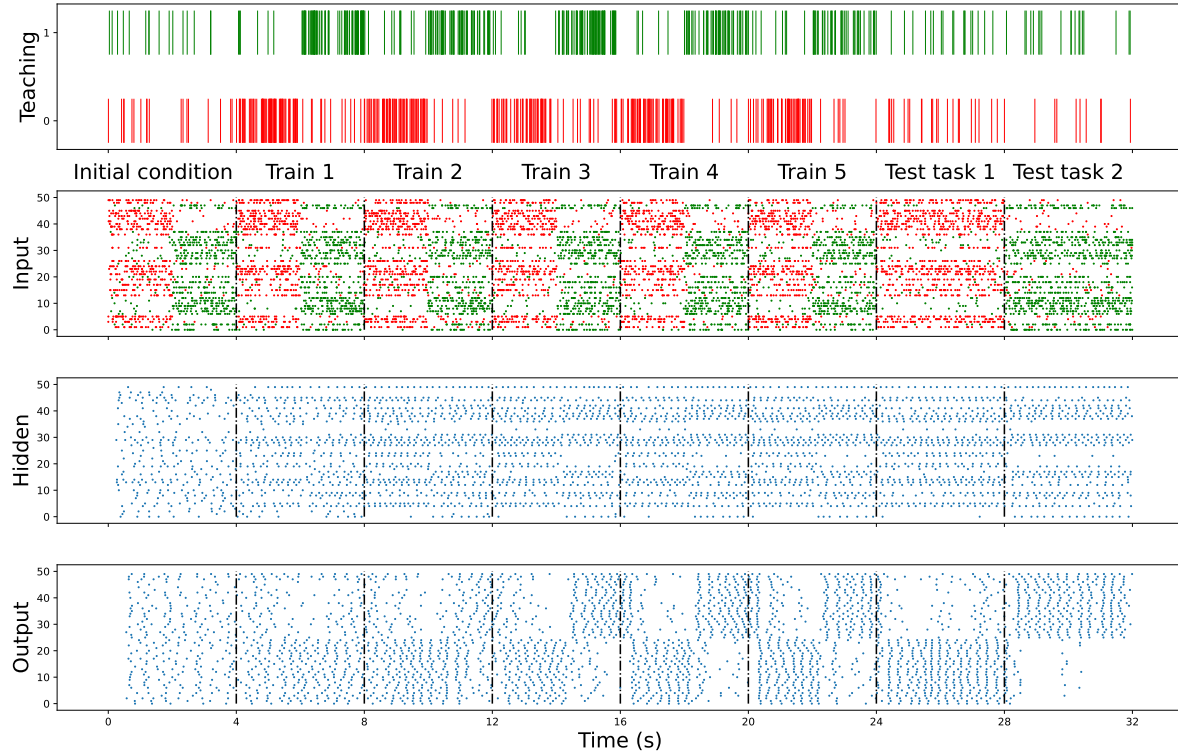


Figure 10: Raster plot of the simulation performed on ARCANA to train a network using ETLP. The first plot represents the spikes of the teaching neurons that are connected to the hidden and output layers. The second plot corresponds to the input pattern, which has two neuron groups that fire with different frequencies. The network has to learn to associate each class with each neuron group. The third and fourth plots are the spikes produced by the hidden and output neurons during the training and testing processes.

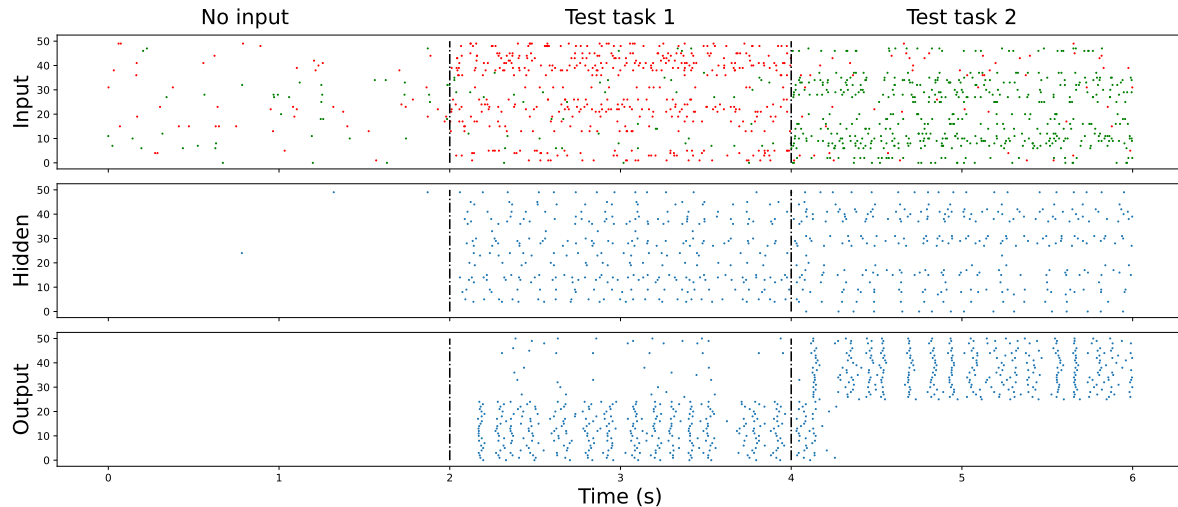


Figure 11: Raster plot of the network running on DYNAP-SE with the weights obtained by training using ETLP

- [4] E. Chicca, F. Stefanini, C. Bartolozzi, and G. Indiveri. “Neuromorphic electronic circuits for building autonomous cognitive systems”. In: *Proceedings of the IEEE* 102.9 (Sept. 2014), pp. 1367–1388. ISSN: 0018-9219. doi: 10.1109/JPROC.2014.2313954.
- [5] Elisabetta Chicca, Fabio Stefanini, Chiara Bartolozzi, and Giacomo Indiveri. “Neuromorphic electronic circuits for building autonomous cognitive systems”. In: *Proceedings of the IEEE* 102.9 (2014), pp. 1367–1388. ISSN: 0018-9219. doi: 10.1109/JPROC.2014.2313954.
- [6] T. Delbruck and A. Van Schaik. “Bias Current Generators with Wide Dynamic Range”. In: *Analog Integrated Circuits and Signal Processing* 43.3 (2005), pp. 247–268.
- [7] Marc-Oliver Gewaltig and Markus Diesmann. “NEST (NEural Simulation Tool)”. In: *Scholarpedia* 2.4 (2007), p. 1430.
- [8] M.L. Hines and N.T. Carnevale. “The NEURON simulation environment”. In: *Neural Computation* 9.6 (1997), pp. 1179–1209.
- [9] G. Indiveri, F. Stefanini, and E. Chicca. “Spike-based learning with a generalized integrate and fire silicon neuron”. In: *International Symposium on Circuits and Systems (ISCAS)*. IEEE. Paris, France, 2010, pp. 1951–1954. doi: 10.1109/ISCAS.2010.5536980.
- [10] Lyes Khacef, Philipp Klein, Matteo Cartiglia, Arianna Rubino, Giacomo Indiveri, and Elisabetta Chicca. “Spike-based local synaptic plasticity: a survey of computational models and neuromorphic circuits”. In: *Neuromorphic Computing and Engineering* 3.4 (Nov. 2023), p. 042001. ISSN: 2634-4386. doi: 10.1088/2634-4386/ad05da. URL: <http://dx.doi.org/10.1088/2634-4386/ad05da>.
- [11] Corey Lammie and Mostafa Rahimi Azghadi. “MemTorch: A Simulation Framework for Deep Memristive Cross-Bar Architectures”. In: *2020 IEEE International Symposium on Circuits and Systems (ISCAS)*. 2020, pp. 1–5. doi: 10.1109/ISCAS45731.2020.9180810.
- [12] Ana Lebanov, Mauricio Velazquez Lopez, Florian De Roose, Nikolas P Papadopoulos, Giacomo Indiveri, Arianna Rubino, Melika Payvand, Steve Smout, Myriam Willegems, Francky Catthoor, et al. “Flexible Unipolar IGZO Transistor-Based Integrate and Fire Neurons for Spiking Neuromorphic Applications”. In: *Biomedical Circuits and Systems, IEEE Transactions on* (2023). doi: <https://doi.org/10.1109/TBCAS.2023.3321506>.
- [13] Carver Mead. “Neuromorphic Engineering: In Memory of Misha Mahowald”. In: *Neural Computation* 35 (2023), pp. 343–383. doi: 10.1162/neco_a_01553.
- [14] Mohammad Javad Mirshojaeian Hosseini, Yi Yang, Aidan J Prendergast, Elisa Donati, Miad Faezipour, Giacomo Indiveri, and Robert A Nawrocki. “An organic synaptic circuit: toward flexible and biocompatible organic neuromorphic processing”. In: *Neuromorphic Computing and Engineering* 2.3 (Sept. 2022), p. 034009. ISSN: 2634-4386. doi: 10.1088/2634-4386/ac830c. URL: <http://dx.doi.org/10.1088/2634-4386/ac830c>.
- [15] S. Moradi, N. Qiao, F. Stefanini, and G. Indiveri. “A Scalable Multicore Architecture With Heterogeneous Memory Structures for Dynamic Neuromorphic Asynchronous Processors (DYNAPs)”. In: *IEEE Transactions on Biomedical Circuits and Systems* 12.1 (Feb. 2018), pp. 106–122. doi: 10.1109/TBCAS.2017.2759700.

- [16] Christian Pehle, Sebastian Billaudelle, Benjamin Cramer, Jakob Kaiser, Korbinian Schreiber, Yannik Stradmann, Johannes Weis, Aron Leibfried, Eric Müller, and Johannes Schemmel. “The BrainScaleS-2 accelerated neuromorphic system with hybrid plasticity”. In: *Frontiers in Neuroscience* 16 (2022), p. 795876.
- [17] Jiale Quan, Zhen Liu, Bo Li, and Jiajun Luo. “Ultra-Low-Power Compact Neuron Circuit with Tunable Spiking Frequency and High Robustness in 22 nm FDSOI”. In: *Electronics* 12.12 (2023). ISSN: 2079-9292. doi: 10.3390/electronics12122648. URL: <http://dx.doi.org/10.3390/electronics12122648>.
- [18] Fernando M Quintana, Fernando Perez-Peña, Pedro L Galindo, Emre O Neftci, Elisabetta Chicca, and Lyes Khacef. “ETLP: event-based three-factor local plasticity for online learning with neuromorphic hardware”. In: *Neuromorphic Computing and Engineering* 4 (3 Aug. 2024), p. 034006. ISSN: 2634-4386. doi: 10.1088/2634-4386/AD6733. URL: <https://iopscience.iop.org/article/10.1088/2634-4386/ad6733%20https://iopscience.iop.org/article/10.1088/2634-4386/ad6733/meta>.
- [19] Malte J. Rasch, Diego Moreda, Tayfun Gokmen, Manuel Le Gallo, Fabio Carta, Cindy Goldberg, Kaoutar El Maghraoui, Abu Sebastian, and Vijay Narayanan. “A Flexible and Fast PyTorch Toolkit for Simulating Training and Inference on Analog Crossbar Arrays”. In: *2021 IEEE 3rd International Conference on Artificial Intelligence Circuits and Systems (AICAS)*. 2021, pp. 1–4. doi: 10.1109/AICAS51828.2021.9458494.
- [20] Ole Richter, Chenxi Wu, Adrian M Whatley, German Köstinger, Carsten Nielsen, Ning Qiao, and Giacomo Indiveri. “DYNAP-SE2: a scalable multi-core dynamic neuromorphic asynchronous spiking neural network processor”. In: *Neuromorphic Computing and Engineering* 4.1 (Jan. 2024), p. 014003. doi: 10.1088/2634-4386/ad1cd7. URL: <https://doi.org/10.1088/2634-4386/ad1cd7>.
- [21] Arianna Rubino, Can Livanelioglu, Ning Qiao, Melika Payvand, and Giacomo Indiveri. “Ultra-Low-Power FDSOI Neural Circuits for Extreme-Edge Neuromorphic Intelligence”. In: *IEEE Transactions on Circuits and Systems I: Regular Papers* 68.1 (2020), pp. 45–56. doi: 10.1109/TCSI.2020.3035575.
- [22] Philipp Spilger, Eric Müller, Arne Emmel, Aron Leibfried, Christian Mauch, Christian Pehle, Johannes Weis, Oliver Breitwieser, Sebastian Billaudelle, Sebastian Schmitt, et al. “hxtorch: PyTorch for BrainScaleS-2: perceptrons on analog neuromorphic hardware”. In: *IoT Streams for Data-Driven Predictive Maintenance and IoT, Edge, and Mobile for Embedded Machine Learning: Second International Workshop, IoT Streams 2020, and First International Workshop, ITEM 2020, Co-located with ECML/PKDD 2020, Ghent, Belgium, September 14–18, 2020, Revised Selected Papers 2*. Springer. 2020, pp. 189–200.
- [23] Marcel Stimberg, Romain Brette, and Dan F.M. Goodman. “Brian 2, an intuitive and efficient neural simulator”. In: *eLife* 8 (Aug. 2019). ISSN: 2050084X. doi: 10.7554/eLife.47314.

- [24] Srikanth Vuppunuthala and Vijay Shankar Pasupureddi. “3.6-pJ/Spike, 30-Hz Silicon Neuron Circuit in 0.5-V, 65 nm CMOS for Spiking Neural Networks”. In: *IEEE Transactions on Circuits and Systems II: Express Briefs* (2023). doi: 10.1109/TCSII.2023.3324584.
- [25] Zhenming Yu, Stephan Menzel, John Paul Strachan, and Emre Neftci. “Integration of physics-derived memristor models with machine learning frameworks”. In: *arXiv preprint arXiv:2403.06746* (2024).
- [26] Dmitrii Zendrikov, Sergio Solinas, and Giacomo Indiveri. “Brain-inspired methods for achieving robust computation in heterogeneous mixed-signal neuromorphic processing systems”. In: *Neuromorphic Computing and Engineering* 3.3 (July 2023), p. 034002. issn: 2634-4386. doi: 10.1088/2634-4386/ace64c. URL: <http://dx.doi.org/10.1088/2634-4386/ace64c>.
- [27] Neta Zmora, Hao Wu, and Jay Rodge. *Achieving FP32 Accuracy for INT8 Inference Using Quantization Aware Training with TensorRT*. <https://developer.nvidia.com/blog/achieving-fp32-accuracy-for-int8-inference-using-quantization-aware-training-with-tensorrt/>. July 2021.

Acknowledgements

F.M.Q. was supported by FPU grant (FPU18/04321) from the Spanish Ministry of Universities.

Competing interests

The authors declare no competing interests.